Received December 7, 2020, accepted December 24, 2020, date of publication January 8, 2021, date of current version January 27, 2021.

Digital Object Identifier 10.1109/ACCESS.2021.3050211

Fault Location in Overhead Transmission Lines Based on Magnetic Signatures and on the Extended Kalman Filter

JÉSUS ANÍCIO DE OLIVEIRA NETO[1], CARLOS ANTONIO FRANÇA SARTORI[2], (Senior Member, IEEE), AND GIOVANNI MANASSERO JUNIOR[3], (Member, IEEE)

[1]Centro Tecnológico da Marinha em São Paulo, São Paulo 05508-000, Brazil
[2]Laboratório de Eletromagnetismo Aplicado, Universidade de São Paulo, São Paulo 05508-010, Brazil
[3]Laboratório de Pesquisa em Proteção e Automação de Sistemas Elétricos, Universidade de São Paulo, São Paulo 05508-010, Brazil

Corresponding author: Jésus Anício de Oliveira Neto (jesus.neto@usp.br)

This work was supported in part by the Coordenação de Aperfeiçoamento de Pessoal de Nível Superior—Brasil (CAPES)—Finance Code 001.

ABSTRACT This paper proposes a non-contact method for fault location in transmission lines, which is based on magnetic fields produced by current signals measured using magnetoresistive sensors installed only at transmission line terminals, under the phase conductors of the first transmission tower at both terminals or at the substations portals. The proposed method uses the Extended Kalman filter to process these measurements and is based on a travelling wave approach in order to perform the fault localization. This paper also describes the implementation and testing of the method, firstly introducing its overview, followed by an analysis of the magnetic fields produced by the current signals, as well as considerations on their measurement; secondly, detailing the Extended Kalman filter and the travelling wave approach; and, finally, presenting the results of the method with regards to simulations built using EMTP/ATP to evaluate its robustness under different conditions varying the fault resistance, fault inception angle, phases involved and fault location. The results indicate that the proposed method is robust and accurate.

INDEX TERMS Electrical fault detection, fault location, Kalman filters, magnetic field measurement, power systems, electromagnetic propagation, signal processing algorithms.

I. INTRODUCTION

A robust and reliable electric power transmission system can guarantee the availability of energy to meet population growth and industrial development, through the interconnection of several electric power generation stations to large urban consumer centers and also to less populated rural regions, constituting large interconnected systems.

These systems are subject to abnormal conditions that may occur in different equipment. However, transmission lines are more susceptible as they cover large areas and, therefore, are more vulnerable to adverse atmospheric conditions, accidents, etc., as in [1].

To ensure power supply with quality, reliability, security and reduced interruption times it is desirable that maintenance crews spend as little time as possible to locate faults and restore operation. For these reasons, algorithms and fault location methods have been proposed in the literature and can be divided into the following main groups, as in [2]–[4]: impedance-based methods; travelling waves; and knowledge-based approaches. The first methods used for fault location in transmission lines were based on the fundamental component of voltages and currents signals [2]. Often referred as impedance calculation methods, these methods relate the fault distance to the impedance of the transmission line, and use measurements of voltage and current signals, provided by voltage transformers (VTs) and/or current transformers (CTs), to perform such calculations, and depend on precise transmission line parameters in order to provide accurate results.

According to [5], fault location algorithms based on impedance calculation may present several error sources, such as: varying loads; remote infeed; fault resistance; mutual coupling; inaccurate line impedances; dc offset and CT saturation; and transmission line topology (e. g. three-terminal lines or tapped radial lines). Several methods were proposed in the literature to overcome these drawbacks, as in [6]–[11]

Methods based on travelling waves (TWs) depend on voltage and current waves propagation and reflection. Whenever a fault occurs, these waves propagate through the

The associate editor coordinating the review of this manuscript and approving it for publication was Bernardo Tellini.

transmission line and reflect back at the two transmission line terminals. The identification of these waves and measurement of their arrival times, associated with the speed propagation of the transmission lines, provide accurate results [12]. This method can be divided into two groups [3], [13]: passive and active methods. Passive methods make use of the transmission line voltages and/or currents TWs to determine the fault distance from the line terminals, while active methods inject high frequency signals in the transmission line whenever a fault occurs, in order to determine the fault location [14].

According to [15] TWs fault location methods: depend on the detection of the fault occurrence instant and the propagation/reflections of the fault signals; usually require high sampling rates, which means that they rely upon sophisticated and costly equipment and upon algorithms with high computational costs; need time synchronization between terminals (for algorithms based on two or more terminal data); and are generally more accurate, when compared to other methods.

The major concerns with regards to such methods are the capability of correctly detecting incident and reflected waves, and also to reduce their dependency on the parameters of the transmission lines. Most of recent research aim towards such goal and, in this context, reference [16] presents a traveling wave fault location method based on directed tree model and linear fitting, which solves the problem of time synchronization, while [17] proposes an accurate method to detected TWs based on the Fast Fourier Transform, and [18] introduces an asynchronous method to avoid the need for synchronization between the transmission line terminals. Besides, [19] presents a fault location method that uses modal transformation and an optimization process that is independent of the line parameters.

Knowledge-based fault location methods are fault tolerant and are capable of generalization. These techniques are inspired in pattern-recognition algorithms and/or decision-making problems. Oftentimes, knowledge-based methods harness features from other fault location methods and from parameters of the transmission lines, as well as high frequency components of the voltage and current signals, to provide inputs to machine-learning approaches that can calculate the fault location.

Usually, these methods present basic fault location schemes which are based on feature extraction processes and artificial intelligence algorithms. Feature extraction processes may rely upon on the Wavelet Transform, as presented in [20], the Discrete Fourier Transform, as in [21], and/or the energy of the signal [22]. The choice of the most suitable artificial intelligence algorithm may consider Artificial Neural Networks, as described in [22], [23], Support Vector Machines, as in [24], Fuzzy Logic, as in [25], and Petri Nets, as in [26].

Overall, knowledge-based methods are customized for particular transmission systems and they need several simulations to provide correct information about the behaviour of these systems. On the other hand, most methods have low computational cost and may present high levels of accuracy.

A. PROPOSED METHOD CONTRIBUTIONS

Most of the techniques presented in the literature require measurements from VTs and/or CTs directly connected to the transmission lines. The main disadvantage of capacitive & coupling capacitor voltage transformer (CVT) and CTs is associated with their performance during transients: while CTs are affected by magnetic core saturation, CVT may suffer from ferroresonance. As a result of saturation, the secondary current is chopped and the accuracy of the measured values is compromised, and as a result of ferroresonance, voltage secondary signals have poor transient response [27]. Therefore, the methods based on such signals may present accuracy issues.

However, it is possible to perform fault location using measurements from equipment installed close to, but not directly connected to transmission lines, in a noninvasive way, as described in [28] and more recently in [29]. Noninvasive approaches have benefits, such as the possibility of locating faults without the need of installing new expensive VTs and CTs, or independently of the position where these equipment are installed.

Magnetic sensors have been studied to monitor power systems for some year, e.g. sensors with anisotropic magnetoresistance [30], giant magnetoresistance [31] and others [32]–[34]. These sensors can provide reliable information for fault detection, classification [35] and location in transmission systems as they avoid CT saturation and other measurement errors that impact the accuracy of some methods.

Reference [28] proposes the design and implementation of a fault location system for overhead transmission lines that is based on non-contact magnetic field sensors installed below the phase conductors of the transmission lines, and the fault location method is based on the detection of changes in the magnitude of the measured magnetic fields at the sensors. The main disadvantage of the proposed method is that it is not cost effective, since it relies on magnetic sensors installed at each transmission tower, on a communication infrastructure that serves all sensors, and on photovoltaic panels to power all of them. Besides, a large number of sensors is necessary, because the detection is based on the magnitude of the magnetic fields in the transmission lines, which is calculated from the root mean square (rms) value of the phase currents, instead of using information about their TW.

Reference [29] presents a non-contact magnetic field-based measurement system which is capable of detecting and locating short-circuit faults in overhead distribution systems. The authors proposal relies on sensors installed along the feeder and its branches and on the analysis of the magnetic fields waveforms for a running window of twenty cycles, whenever a low impedance fault occurs. The proposed procedure reads sensors data and determine the peak values of the magnetic fields at each measuring point, and determine the fault

location using the assumption that the distribution network is radial. The main disadvantage of this procedure is that it is specific for radial distribution systems and cannot be used to determine the fault location in transmission lines without modifications, besides, it is used only to determine low impedance faults and it relies on a costly infrastructure of sensors and a communication infrastructure.

Reference [36] proposes a fault location system based on non-contact magnetic field measurements and on an autoregressive modeling of the magnetic signature measured around the transmission line. The approach lacks the capability of self-adjusting in order to cope with typical variations of the magnetic fields as a result of load variations (variations of changes resistive, reactive and apparent power), topology changes (circuit-breaker and/or switchgear maneuvers), etc.

Therefore, this paper proposes an approach, based on non-contact magnetic fields measurements for fault location in transmission lines, measured using magnetoresistive sensors installed only at transmission line terminals, under the phase conductors of the first transmission tower at both terminals or at the substations portals. The proposed method uses the Extended Kalman filter to process these measurements and is based on a travelling wave approach in order to perform the fault localization. Due to the use of the Extended Kalman filter (EKF), that estimates the magnetic field behaviour in the vicinity of the transmission line terminals, the proposed method is self-adaptive and is capable of detecting the fault occurrence when the difference between the measured magnetic fields and their estimation surpass a predefined, and also self-adaptive, threshold. Besides it copes well with noisy input signals.

B. MANUSCRIPT STRUCTURE

The rest of the paper is divided as follows: section II presents the fault location method proposed by the authors, with respect to its theory and application to the fault location problem; section III presents details regarding its implementation and configuration when used to locate faults in a simulated system; section IV presents a statistical analysis of the method, as well as considerations of its performance when tested against circa ten thousand simulations varying fault resistance, inception angle, distance, phases involved and fault type; and section V presents the authors conclusions.

II. FAULT LOCATION METHOD

The fault location method proposed in this paper combines information provided by two sets of hardware-based magnetoresistive sensors installed only at transmission line terminals, under the phase conductors of the first transmission tower at both terminals or at the substations portals with an algorithm that is based on the type D TW fault location [3], and information provided by the intelligent electronic devices (IEDs) responsible for isolating the fault in the transmission line (TL), as depicted in Fig. 1.

These sensors [37] have the capability to capture the magnetic field produced by the phase currents, process, and output information over a communication network to the

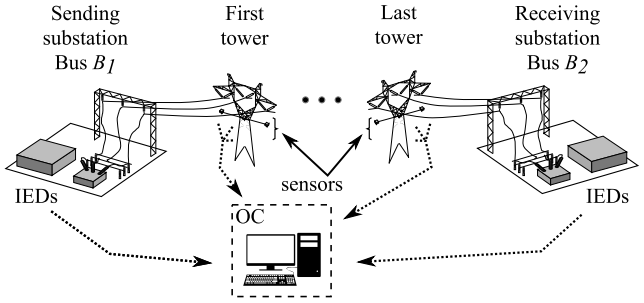

FIGURE 1. Fault location infrastructure.

operation center. To process this information, the sensors use a method based on the Extended Kalman filter (EKF) that is able to detect when an overcurrent event occurs by detecting abnormalities whenever the errors between measured magnetic fields and the prediction of the model for the same fields exceed predefined limits.

When this occurs, the sensors send this information to the operation center where the fault localization is performed. The fault localization algorithm is based on the type D traveling wave fault location technique and whenever a fault within the protection zone is detected by the protective devices the location is provided to the engineers at the operation center.

The next sections (II-A, II-B, and II-C) present considerations about the magnetic field measurements, details on the EKF theory and application, and the fault location *per se*.

A. MAGNETIC FIELD MEASUREMENTS

Currents circulating along conductors produce a magnetic field that can be decomposed into two spatial components [38]: vertical $H_x(k)$ and horizontal $H_y(k)$. According to Ampere's circuital law, the magnetic field can be described as in

$$\vec{H}(k) = H_x(k) \cdot \hat{a}_x + H_y(k) \cdot \hat{a}_y \tag{1}$$

where

$$H_x(k) = \sum_{n=1}^{3} D_n \cdot i_n(k), \quad \text{and } H_y(k) = \sum_{n=1}^{3} Q_n \cdot i_n(k) \tag{2}$$

$\hat{a}_x$ and $\hat{a}_y$ are vectors of x and y axes, n is the number of the conductor ($n = 1, 2$ and 3), and $i_n(k)$ is the k^{th} sample of the current signal circulating in conductor n. Spatial sensor dispositions regarding conductor n are

$$D_n = \frac{d_{y,n}}{2\pi \cdot R_n^2} \quad \text{and } Q_n = \frac{d_{x,n}}{2\pi \cdot R_n^2} \tag{3}$$

where $d_{x,n}$, $d_{y,n}$, and $R_n = \sqrt{d_{x,n}^2 + d_{y,n}^2}$ are the horizontal, vertical, and linear distances between the sensor and conductor n, respectively, as depicted in Fig. 2.

Equation (1) describes the superposition of the magnetic field contributions of each conductor on the horizontal and vertical axes. This way, the squared absolute value of the magnetic field can be obtained as in

$$H^2(k) = H_x^2(k) + H_y^2(k) \tag{4}$$

Signals $H_x(k)$ and $H_y(k)$ inherit the sinusoidal behavior and frequency of the transmission line currents signals. By raising

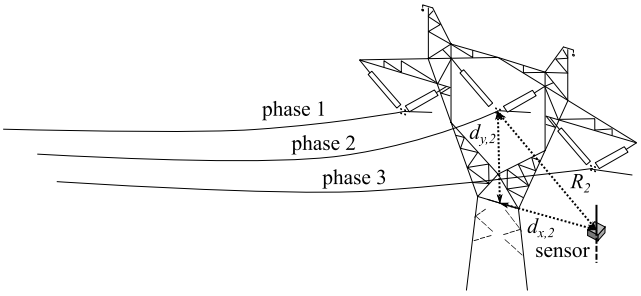

FIGURE 2. Sensor positioning.

the magnetic field to square, i. e. $H_x(k)^2$ and $H_y(k)^2$ the signals frequencies double and a dc component appears. The EKF proposed in this paper uses these squared signals.

B. EXTENDED KALMAN FILTER

Kalman filtering is used for many applications (e. g., evaluation of harmonic distortion, minimization of measurement noise and disturbance detection [39], [40]). It consists of a group of state-space equations, which contains information about the behaviour of the observed system, and is capable of estimating approximate measurements of it using actual measurements recorded over time.

The proposed method is based on the EKF, associated with a complex sinusoidal signal, using the *Euler* formulation. Therefore, the complex sinusoidal signal is represented [1] as in

$$a\cdot\sin(k\cdot w\cdot T_s+\phi)=a\cdot\frac{e^{j\cdot(kwT_s+\phi)}-e^{j(-kwT_s-\phi)}}{2j} \tag{5}$$

where a is the amplitude of the sinusoidal signal, k is the k$^{\text{th}}$ sample, T_s is the complex sinusoidal signal sample period, w is its angular frequency, ϕ is its angle, and $j=\sqrt{-1}$.

From the definition

$$\begin{cases} u(k) = a\cdot e^{j\cdot(k\cdot w\cdot T_s+\phi)} \\ u(k)^* = a\cdot e^{j\cdot(-k\cdot w\cdot T_s-\phi)} \\ \alpha = e^{j\cdot w\cdot T_s} \end{cases} \tag{6}$$

In order to correctly represent the operation of the system, the authors considered the three-state model to allow variation of amplitude, phase, and frequency,[2] represented by $|u(k)|$, $\angle u(k)$, and $\angle\alpha$, respectively. Therefore, it is possible to describe the complex sinusoidal signal in a state-space representation, as in

$$\underbrace{\begin{bmatrix}\alpha\\ u(k+1)\\ u(k+1)^*\end{bmatrix}}_{\mathbf{x}(k+1)} = \underbrace{\begin{bmatrix}1&0&0\\0&\alpha&0\\0&0&\alpha^{-1}\end{bmatrix}\times\underbrace{\begin{bmatrix}\alpha\\ u(k)\\ u(k)^*\end{bmatrix}}_{\mathbf{x}(k)}}_{\mathbf{f}(\mathbf{x}(k))} + v(k) \tag{7}$$

where $\mathbf{x}(k+1)$ and $\mathbf{x}(k)$ are the k$^{\text{th}}+1$ and k$^{\text{th}}$ samples of the intermediate state, respectively, and $v(k)$ is the k$^{\text{th}}$ process noise.

[1] Nonlinear sinusoidal state-space representation of electric power signals may have different approaches, and the estimation of phase and frequency of such signals is discussed in [40], [41]

[2] The frequency state contributes to fast EKF accommodation in the event of states variations.

The signal measurement is represented as in

$$z(k)=\underbrace{\begin{bmatrix}0 & \frac{1}{2\cdot j} & -\frac{1}{2\cdot j}\end{bmatrix}}_{\mathbf{H}}\times\mathbf{x}(k)+w(k) \tag{8}$$

where $w(k)$ is the k$^{\text{th}}$ measured noise.

It is possible to estimate a complex sinusoidal signal from the linearization of the system described in eqs. (7) and (8) and then using a recursive nonlinear filter [42]. The estimation is divided into three steps: initialization, prediction and update, and these steps are described in sections II-B1, II-B2 and II-B3.

1) INITIALIZATION

The model estimation step starts with correctly choosing the initial parameters of the EKF, as it accelerates the filter convergence. Consequently, the authors decided to normalize the square of magnetic field captured by the sensors to remove its dc offset and to provide unitary amplitude, facilitating the initialization of further terms. The proposed normalization uses the maximum $\left(H_M^2\right)$ and minimum $\left(H_m^2\right)$ values of the squared fields, as in

$$z(k)=2\cdot\frac{H^2(k)-H_m^2}{H_M^2-H_m^2}-1 \tag{9}$$

It is important to mention that the procedure to remove the dc offset that appears due to the squared value of the magnetic field also removes the dc offset that appears due to the geomagnetically induced currents driven by the geomagnetic field disturbances, since for electrical networks operating at industrial frequency (e. g. 50Hz or 60Hz), these currents behave as direct currents, not varying in time [43], [44].

In addition to this procedure, the initial state-space matrix is defined, as in

$$\hat{\mathbf{x}}(0)=\left[e^{j\cdot(w_0\cdot T_s)} \quad a_0\cdot e^{j\cdot(w_0\cdot T_s+\phi_0)} \quad a_0\cdot e^{j\cdot(-w_0\cdot T_s-\phi_0)}\right]^T \tag{10}$$

where w_0 is the initial angular speed of $z(k)$ signal, a_0 is the maximum amplitude of it, and ϕ_0 is the initial angle.

The angular speed w_0 is equal to $2\cdot\pi\cdot 120\ \frac{rad}{s}$ and the amplitude $a_0=1$, since the signal is normalized according to (9). To determine ϕ_0, it is necessary to use the first sample of $z(k)$ and proceed as in

$$\phi_0=\sin^{-1}(z(1))-2\cdot\pi\cdot w_0\cdot T_s \tag{11}$$

It is important to mention that the initialization at each line terminal is performed independently. Therefore, each squared magnetic field has its own initialization matrix.

After the filter initialization, measurements of the magnetic fields are performed over a limited time interval. This interval is required to improve the filter stability before proceeding to the next step.

2) PREDICTION

This step predicts the output of the nonlinear system at discrete-time instant $t(k)$, given the state estimation at

discrete-time instant $t(k-1)$ as in

$$\hat{\mathbf{x}}(k)^{-} = \mathbf{f}\left(\hat{\mathbf{x}}(k-1)\right) \tag{12}$$

where the "$^-$" signal represents the current estimate given previous measurements (e. g. estimate $\hat{\mathbf{x}}(k)^{-}$ is predicted using $\mathbf{x}(k-1)$).

3) UPDATE

This step corrects the estimation of the previous step, as in

$$\hat{\mathbf{x}}(k) = \hat{\mathbf{x}}(k)^{-} + \mathbf{K}(k) \times \left\{z(k) - \mathbf{H} \times \hat{\mathbf{x}}(k)^{-}\right\} \tag{13}$$

and, finally, estimates the measured value as in

$$\hat{z}(k) = \mathbf{H} \times \hat{x}(k) \tag{14}$$

where the optimal value of the EKF gain matrix is calculated as in

$$\mathbf{K}(k) = \mathbf{P}(k)^{-} \times \mathbf{H}^{T} \times \left\{\mathbf{H} \times \mathbf{P}(k)^{-} \times \mathbf{H}^{T} + \mathbf{R}\right\}^{-1} \tag{15}$$

The calculation of the EKF gain matrix depends on the measurement noise covariance matrix ($\mathbf{R}$) and on the prediction of the error covariance matrix ($\mathbf{P}$).

The initialization of the error covariance matrix depends on the identity matrix, i.e., $\mathbf{P}(0)^{-} = \mathbf{I}$, and its prediction is based on two matrices: the Jacobian matrix ($\mathbf{F}$) and the process noise covariance matrix ($\mathbf{Q}$) as in

$$\mathbf{P}(k)^{-} = \mathbf{F}(k-1) \times \mathbf{P}(k-1) \times \mathbf{F}(k-1)^{T} + \mathbf{Q} \tag{16}$$

where

$$\mathbf{F}(k-1) = \begin{bmatrix} 1 & 0 & 0 \\ \hat{u}(k-1) & \alpha & 0 \\ \dfrac{-\hat{u}(k-1)^{*}}{\alpha^{2}} & 0 & \dfrac{1}{\alpha} \end{bmatrix} \tag{17}$$

Then, matrix $\mathbf{P}$ is corrected, as in

$$\mathbf{P}(k) = \{\mathbf{I} - \mathbf{K}(k) \times \mathbf{H}\} \times \mathbf{P}(k)^{-} \tag{18}$$

With regards to matrices $\mathbf{Q}$ and $\mathbf{R}$, the authors assumed that the model rigorously describes the process and decided to choose them in accordance to [45]. Then

$$\mathbf{Q} = 0\%, \quad \text{and } \mathbf{R} = 3\% \tag{19}$$

C. IMPLEMENTATION OF THE PROPOSED METHOD

The fault location method proposed in this work is based on three steps, as depicted in Fig. 3: system initialization, real time cyclic execution and fault location. These steps are described in sections II-C1, II-C2 and II-C3.

1) INITIALIZATION

a: NORMALIZATION PARAMETERS CALCULATION

During the initialization step the proposed method uses a data window of Δt_M seconds to determine the typical minimum $\left(H_m^2\right)$ and maximum $\left(H_M^2\right)$ values of $H^2(k)$, as in

$$\begin{cases} H_m^2 = \min\left\{H^2(k-k_M, k)\right\} \\ \\ H_M^2 = \max\left\{H^2(k-k_M, k)\right\} \end{cases} \tag{20}$$

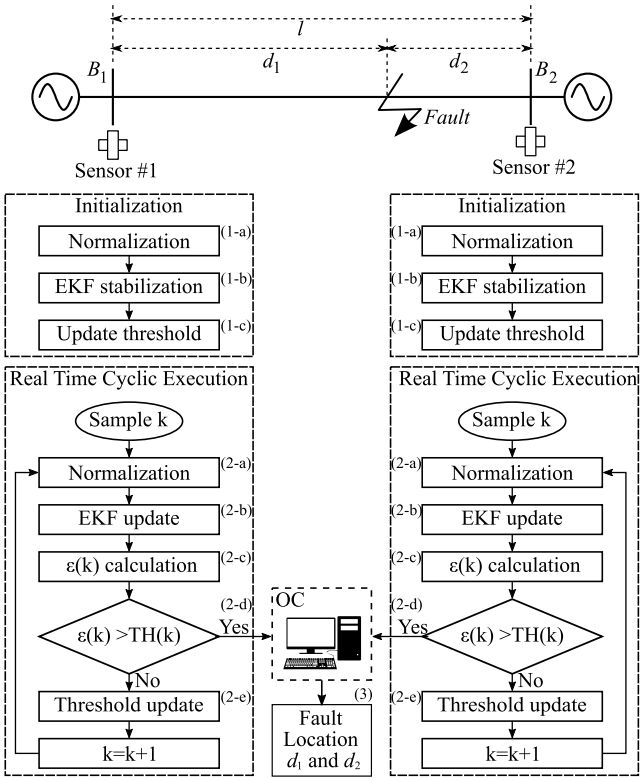

FIGURE 3. Fault location system.

where $k_M = \frac{\Delta t_M}{T}$ and T is the sampling period. This parameter allows to normalize all $H^2(k)$ samples as proposed in section II-B1 and in (9).

b: MODEL STABILIZATION

The same Δt_M data window is used for the EKF model to gain stability. The first sample of this data window is used to initialize the EKF model and after that, EKF estimates $\hat{z}(k)$ for each normalized sample $z(k)$, as presented in sections II-B2 and II-B3.

c: THRESHOLD INITIALIZATION

The threshold value consists of the maximum absolute error between the estimated and normalized values, within a Δt_N data window, that is used to determine if a disturbance in the magnetic fields has occurred. The estimation error is calculated as in

$$\varepsilon(k) = |\hat{z}(k) - z(k)| \tag{21}$$

and the threshold (TH) is calculated as in

$$\mathrm{TH}(k+1) = K_g \cdot \max\left\{\varepsilon(k-k_N, k)\right\} \tag{22}$$

where $\hat{z}(k)$ and $z(k)$ are the k$^{\text{th}}$ samples of the estimated and normalized signals, respectively, as described in section II-B, K_g is an arbitrary constant, $\max\{\varepsilon(k-k_N, k)\}$ is the maximum value of ε within the data window of Δt_N, and $k_N = \frac{\Delta t_N}{T}$.

It can be noticed that during the initialization step, the fault location function is blocked in order for the proposed method to gain stability and determine the initial threshold.

The minimum time interval of this step is $\Delta t_M + \Delta t_N$. Then, the next step is the real time cyclic execution.

2) REAL TIME CYCLIC EXECUTION

The real time cyclic execution consists of five steps, as follows.

a: NORMALIZATION

Each new $H^2(k)$ calculated by the sensor is normalized according to (9) by the min-max values H_m^2 and H_M^2 calculated at step 1, producing a new $\hat{z}(k)$.

b: ESTIMATION AND UPDATE

This procedure is described in section II-B.

c: ESTIMATION ERROR CALCULATION

The proposed method calculate the absolute error between the EKF estimated signal $\hat{z}(k)$ and the normalized signal $z(k)$ whenever there is a new sample, as in (21).

d: THRESHOLD COMPARISON

Then, it compares the absolute error to the threshold, calculated as in (21) and (22), respectively. A disturbance is detected when

$$\varepsilon(k) > \mathrm{TH}(k) \tag{23}$$

The instant when the disturbance is detected at both transmission line terminals is sent to the computer at the operation center, that is responsible for the fault location, as described in II-C3.

e: THRESHOLD UPDATE

After the model estimation, the proposed method updates the detection threshold based on the estimation error $\varepsilon(k)$. To accomplish this, the proposed method uses another Δt_N data window positioned before the k$^{\text{th}}$ sample. The threshold is calculated as in (22).

3) FAULT LOCATION

When a disturbance is detected, the information about the disturbance instant, detected at both transmission line terminals, are sent to the operation center, where the fault distance is estimated using the traveling wave theory [3], [46]. Considering the transmission line depicted in Fig. 3, it is possible to locate the fault point, as in

$$d_1 = \frac{l - v \cdot \Delta t_F}{2} \quad \text{and} \quad d_2 = \frac{l + v \cdot \Delta t_F}{2} \tag{24}$$

where l is the total length of the transmission line, v is the TW speed at the transmission line, $\Delta t_F = t(k_2) - t(k_1)$ is the time difference between the two disturbance instants at line terminals B_1 and B_2, respectively, and t is the sampling instant. Therefore, k_1 and k_2 are the samples when the disturbance is detected, while d_1 and d_2 are the distances between the fault point and the same line terminals, respectively.

An accurate estimation of Δt_F is required to exactly find the fault occurrence point. Therefore, there must time synchronization between sensors at each line terminal, and this requirement can be met by using Global Positioning System (GPS) time synchronization, associated with time protocols such as: Precision Time Protocol (PTP), Inter-Range Instrumentation Group - Time Code Format B (IRIG-B), etc.

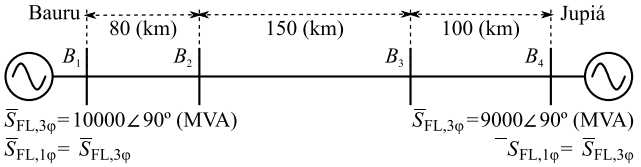

FIGURE 4. 440 kV system.

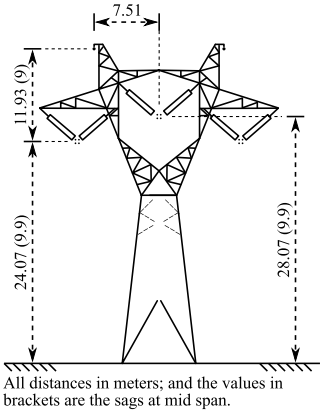

FIGURE 5. Tower geometries of 440 kV system.

The correct information about propagation speed is important, since it impacts the precision of not only the method proposed in this paper, but all methods based on TW (the proposed method presents a maximum theoretical error of $\frac{x}{2}\%$ in the fault occurrence point calculation when there is an error of $x\%$ in the propagation speed). Besides, to account for mutual coupling between phases and nearby lines in the calculation of the propagation speeds in the phase conductors, it is possible to use the procedure described in [47].

III. APPLICATION EXAMPLE

This section details the transmission system used to validate the proposed method, presents an analysis of the magnetic field behaviour around the transmission line that is part of this system and describes the result of the proposed method when locating a three-phase fault.

A. ELECTRIC SYSTEM DESCRIPTION

The system used to validate the proposed method consists of a 440 kV transmission system owned by Companhia de Transmissão de Energia Elétrica Paulista (São Paulo Electric Power Transmission Company) – CTEEP, that connects Bauru and Jupiá substations, as illustrated in Fig. 4. It also depicts the fault levels at the transmission line terminals and the line length.

The tower geometry is illustrated in Fig. 5 and Table 1 presents information about the phase conductors and ground wires. The propagation speed values for this transmission line is $v_{440} = 295045 \frac{km}{s}$ (propagation speed is close to the light speed).

TABLE 1. Transmission lines conductors data.

Conductor	External radius (mm)	Internal radius (mm)	Resist. $\left(\frac{\Omega}{\text{km}}\right)$
Phase	12.570	4.64	0.08998
Ground wire	4.572	–	4.188

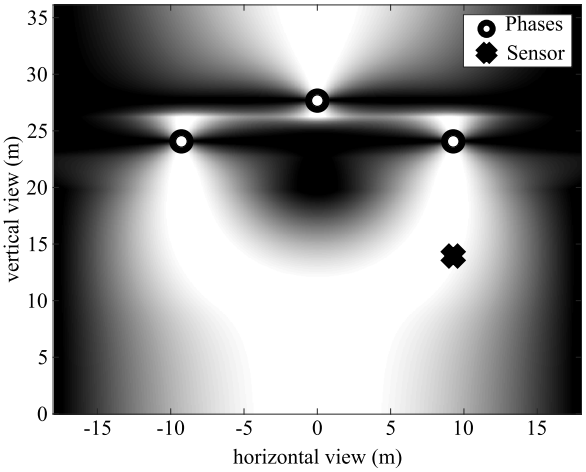

FIGURE 6. Magnetic field spatial distribution at the transmission line in a cross-sectional view.

The authors used electromagnetic transient program (EMTP) to implement this transmission system and the support routine LINE CONSTANTS to calculate the transmission line parameters.

B. MAGNETIC FIELD MEASUREMENT

This section presents an analysis of the magnetic field at the transmission system due to the influence of the three-phase currents that circulate in the transmission line. This analysis allowed the authors to properly position the sensors, as presented in section III-B1, and to evaluate the influence of the chosen position in the accuracy of the proposed method, as presented in section III-B2.

1) SENSORS SPATIAL DISTRIBUTION

The spatial distribution of the magnetic field intensity around the transmission system in normal operation, as depicted in a cross-sectional view in Fig. 6, was used to correctly distribute the sensors. Axis x corresponds to the horizontal coordinate, considering the central conductor in the coordinate $x = 0$, and axis y represents the vertical coordinate, considering $y = 0$ the coordinate of the ground. Fig. 7 illustrates the cross-sectional view of the sensors under the transmission line conductors (the sensor position is marked with "X" and the phase cables representation are marked with "O").

After some trial and error attempts to position the sensor, the authors recommend: a) placing the sensors in the higher field intensity to increase the sensor signal-to-noise ratio; b) avoiding the equidistant distance between the sensor and the phase conductors, since the sensor may not correctly measure the current variations. This is due to the fact that there may be magnetic field cancellations (manly with regards to high impedance faults); c) other arrangements are possible and Figs. 6 and 7 represent only one of them.

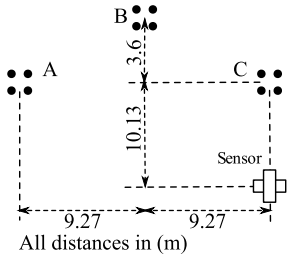

FIGURE 7. Sensors spatial arrangements.

It is important to mention that the sensors architecture the technique involved in their construction, as well as the methods available for the collection and analysis of data processed by them, decisively affect the accuracy of the fault location methods that use these technologies. References [48] and [49] discuss these issues in more detail.

2) DISTANCE FROM THE SENSOR TO THE TRANSMISSION LINE

The distance from the phase conductors to the sensor may introduce errors in the proposed method, since the magnetic fields propagate in this space. Thus, the magnetic field that leaves a phase conductor n presents a time delay (t_{ns}) at the sensor s, i. e.

$$\vec{H}_s(t) = \vec{H}_n(t + t_{ns}) \tag{25}$$

where $\vec{H}_n(t)$ is the magnetic field that leaves conductor n and $\vec{H}_s(t)$ is the magnetic field that is measured by sensor s.

Considering (24) and the propagation of the magnetic fields from the phase conductors to the sensor, it is possible to calculate the estimated distance of the fault as in

$$\hat{d}_1 = d_1 + \frac{d_{ns1} - d_{ns2}}{2} \tag{26}$$

where d_{ns1} is the distance from a sensor at one terminal of the transmission line to one of the phase-conductors, and d_{ns2} is the distance from a sensor at the other transmission line terminal to the same conductor. It can be noticed (26), that if the distance from the phase conductor to the sensor is the same at both line terminals ($d_{ns} = d_{ns1} = d_{ns2}$), the estimated distance ($\hat{d}_1$) is equal to the real distance $\left(\hat{d}_1 = d_1\right)$.

In practice, it is difficult to obtain such precision during the sensors installation, and considering that the maximum precision is 1 m, the maximum error would be

$$\varepsilon_{ns} = \frac{(d_{ns} + 1) - (d_{ns} - 1)}{2} = 1 \text{ m} \tag{27}$$

The error caused by the sensor position is not substantial when compared to the transmission line length. Therefore, the authors decided to consider that the sensors at both transmission line terminals were precisely installed. The simulations considered that both sensors were hypothetically installed near terminals B_2 and B_3 of the 440 kV transmission system.

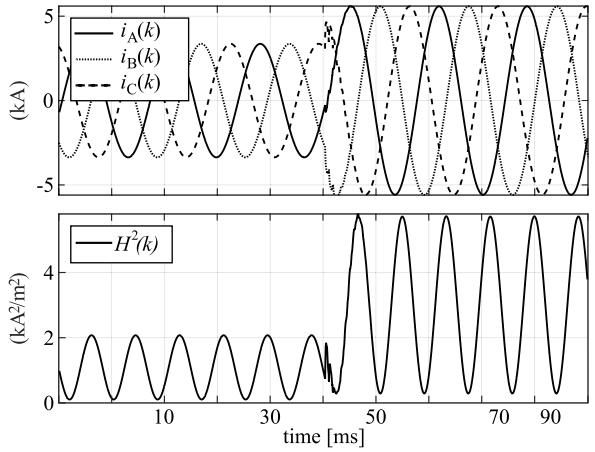

FIGURE 8. Three-phase currents and $H^2(k)$ signal at terminal B_2 of the 440 kV system.

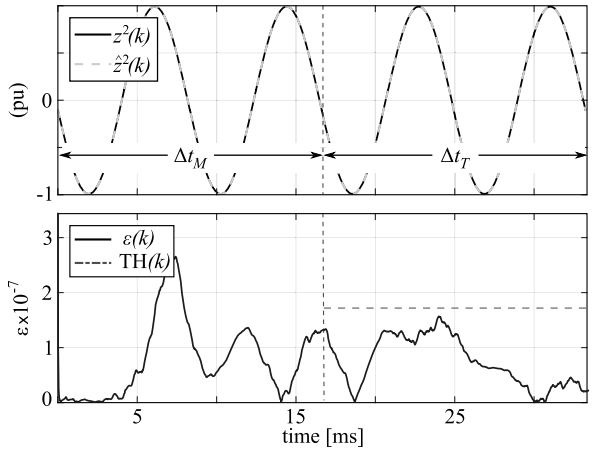

FIGURE 9. Stabilization, error and threshold calculation at terminal B_2 of the 440 kV system.

C. APPLICATION AND SETTINGS OF THE PROPOSED METHOD

This section describes the results of the proposed method for a three-phase fault in the 440 kV system, 100 km from terminal B_2. Fig. 8 illustrates the three-phase currents plus the $H(k)^2$ signal.

As previously mentioned, the fault location method proposed in this work is based on three steps: initialization, real-time cyclic execution and fault location. The following sections describe the behaviour of the algorithm with regards to the three-phase fault.

1) INITIALIZATION

a: NORMALIZATION PARAMETERS CALCULATION

Firstly, the method calculates the normalization parameters and performs the signal normalization, producing a $z(k)$ signal.

b: MODEL STABILIZATION

Then, it defines the initial state matrix $\hat{\mathbf{x}}(0)$, as in (10), calculates the angle of the normalized signals at both terminals, as in (11), and obtains $\phi_0^{B_2} = -3.031$ rad and $\phi_0^{B_3} = -3.113$ rad.

Considering the sampling frequency as $f_s = 1.5$ MHz and the initial frequency as $w_0 = 2 \cdot \pi \cdot 120 \ \frac{\text{rad}}{\text{s}}$, it is possible to calculate the initial state matrix for each line terminal, used to calculate $\hat{z}(k)$, as in

$$\hat{\mathbf{x}}(0)\Big|_{B_2} = \begin{bmatrix} 0.\overline{9} + 0.005 \cdot j \\ -0.994 - 0.\overline{1} \cdot j \\ -0.994 + 0.\overline{1} \cdot j \end{bmatrix} \tag{28}$$

$$\hat{\mathbf{x}}(0)\Big|_{B_3} = \begin{bmatrix} 0.\overline{9} + 0.005 \cdot j \\ -0.\overline{9} - 0.029 \cdot j \\ -0.\overline{9} + 0.029 \cdot j \end{bmatrix} \tag{29}$$

The decision to use a sampling frequency of $f_s = 1.5$ MHz is related to the expected precision of the method, as it depends on the sampling frequency and the propagation speed of the transmission system [3], [46]. The precision for a TW method due to sampling frequency can be calculated for the simulated system and is $\Delta d_{440} = \frac{v_{440}}{2 \cdot f_s} = 98.3$ m.

c: THRESHOLD INITIALIZATION

After the EKF stabilization, which takes a time interval of $\Delta t_M = \frac{2}{120}$ s, the proposed method calculates the threshold at both transmission line terminals, using the maximum estimation error calculated as in (21) and (22), within a data window of $\Delta t_T = \frac{2}{120}$ s. Fig. 9 illustrates the threshold initialization on terminal B_2 for terminals B_2.

To determine both windows (Δt_M, Δt_T) the proposed method considers two periods of the fundamental frequency (120 Hz in the simulation cases - nominal frequency of H^2 - or a period of 60 Hz). The K_g parameter requires a value above the value of the steady state error (the authors decided to use an arbitrary value of 10% above the steady state error, because it was possible to perform an accurate detection without security errors when there are abrupt variations in the system, such as load variations, for instance). This parameter must be adjusted for actual installations in order to provide the best compromise between security and precision of the fault location.

The initial thresholds at the line terminals B_2 and B_3 are 1.84×10^{-7} and 2.01×10^{-7}, respectively.

2) REAL TIME CYCLIC EXECUTION

After the system initialization step, the real time cyclic execution starts, and: 2-a) each new sample is normalized, 2-b) the EKF is updated and estimates $\hat{z}(k)$, 2-c) the estimation error is calculated, 2-d) the maximum estimation error is compared to the threshold, 2-e) the threshold is updated, and 2-f) the detection occurs when the estimation error crosses the adaptive threshold, calculated in the previous stage.

Figures 10 and 11 illustrate the signals estimated by the EKF as well as the absolute error between the estimated values and the actual ones at line terminals B_2 and B_3, respectively. It is also noticed that the EKF error converges to a value of 10^{-8} due to signal normalization. This is because the signal normalization (9) does not completely eliminate the dc offset.

TABLE 2. Results of the location algorithms - inception angle.

FT	Inception Angle (°)											
	0	30	60	90	120	150	180	210	240	270	300	330
	Absolute Error (m)											
AG	33	42	31	1	11	21	9	53	15	35	7	54
BG	23	32	4	11	40	57	4	42	10	22	23	2
CG	6	1	10	20	42	30	15	19	1	27	27	51
AB	19	32	10	13	20	42	36	54	14	50	44	40
BC	22	3	9	16	20	15	28	41	38	35	14	41
CA	31	8	37	36	56	17	22	18	17	23	6	26
ABG	37	13	42	30	24	22	17	57	14	29	11	11
BCG	24	11	36	31	26	29	57	29	36	9	9	1
CAG	10	36	20	11	40	45	50	26	23	4	6	6
ABC	47	33	20	24	30	28	10	24	25	50	37	34
μ	25	21	22	19	31	31	25	36	19	28	18	26
σ	12	14	13	10	13	13	17	14	11	14	13	19

FT = Fault type, μ= Mean absolute squared error, σ = Standard deviation

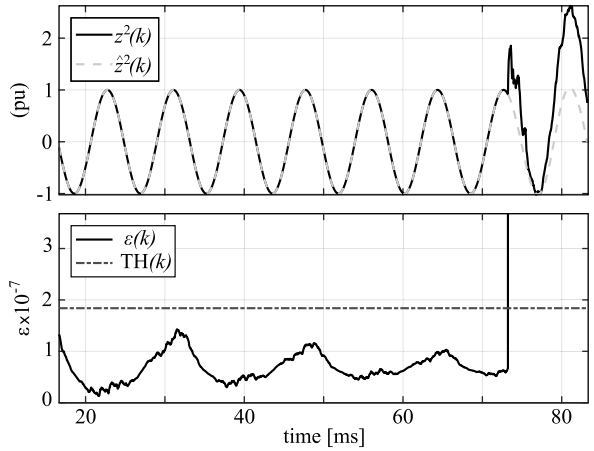

FIGURE 10. Error estimation and threshold at terminal B_2 of the 440 kV system.

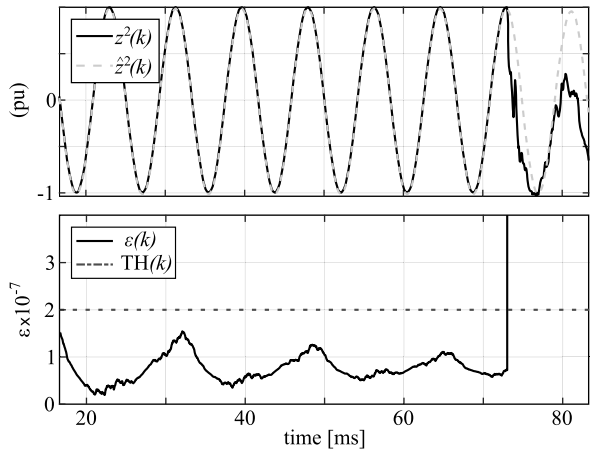

FIGURE 11. Error estimation and threshold at terminal B_3 of the 440 kV system.

3) FAULT LOCATION

As depicted in both figures, the estimation error at line terminal B_2 crosses the threshold at instant $t(k_1) = 73.7880$ ms, while at line terminal B_3 it crosses at $t(k_2) = 73.6187$ ms, therefore, $\Delta t_F = -0.1693$ ms. Considering that the wave propagation speed is v_{440} and the total line length is $l = 150$ km, the estimated fault distance is $d_1 = 99.98$ km, which presents a location error of only 20 m.

IV. STATISTICAL ANALYSIS AND COMPARISON

In order to perform a thorough investigation of the proposed method, the authors decided to evaluate its behaviour with respect to different fault inception angles, fault resistances and distances. As a result, the authors simulated ten thousand random situations to assess the overall effectiveness of the proposed method using EMTP. The values used in these simulations were:

- Fault inception angles: from $0° \leq \theta_f \leq 360°$;
- Fault resistance: $0 \leq R_f \leq 300\ \Omega$;
- Fault distance: 5 km $\leq D_f \leq$ 145 km; and
- Fault type and phases involved: AG, BG, CG, AB, BC, CA, ABG, BCG CAG, and ABC;

A. INCEPTION ANGLE ANALYSIS

Table 2 presents the results of 120 simulations used to analyse the effectiveness of the proposed method with respect to the fault inception angle and fault type (the other parameters were randomly selected).

It can be noticed that the inception angle has no direct relation to the accuracy of the method. The worst case presents an error of 57 m, and it occurs for a BCG fault with a fault resistance of 46 Ω, a fault inception angle of 180°, and at a fault distance of 143 km. Besides, the maximum error is less than the accuracy of the method due to the sampling frequency (please refer to section III-C1.b for more details).

B. FAULT RESISTANCE ANALYSIS

Table 3 presents the results of 60 simulations used to analyse the effectiveness of the proposed method with respect to the fault resistance and fault type (the other parameters were randomly selected).

It can be noticed that the fault resistance has no direct relation to the accuracy of the method. The worst case presents an error of 57 m, and it occurs for a CA fault with fault resistance of 10 Ω, fault inception angle of 270°, and at a fault distance of 12 km. As mentioned before, the maximum error is less than the accuracy of the method due to the sampling frequency (please refer to section III-C1.b for more details).

C. FAULT DISTANCE ANALYSIS

Table 4 presents the results of 80 simulations used to analyse the effectiveness of the proposed method with respect to the

TABLE 3. Results of the location algorithms - fault resistance.

FT	Fault resistance (Ω)					
	0	10	50	100	200	300
	Error (m)					
AG	24	40	7	12	8	2
BG	1	38	31	23	44	36
CG	3	41	40	22	18	21
AB	26	18	24	38	14	19
BC	53	13	37	48	33	24
CA	15	57	24	14	9	19
ABG	5	8	40	21	53	40
BCG	25	33	44	24	37	26
CAG	51	2	1	33	48	53
ABC	33	17	29	8	31	8
μ	23	27	28	24	30	25
σ	17	17	14	12	15	14

FT = Fault type, μ= Mean absolute squared error, σ = Standard deviation

TABLE 4. Results of the location algorithms - fault distance.

FT	Fault distance (km)							
	5	25	45	65	85	105	125	145
	Error (m)							
AG	24	39	4	32	32	4	39	24
BG	24	39	4	32	32	4	39	24
CG	24	39	4	32	32	4	39	24
AB	24	39	4	32	32	4	39	24
BC	24	39	4	32	32	4	39	24
CA	24	39	4	32	32	4	39	24
ABG	24	39	4	32	32	4	39	24
BCG	24	39	4	32	32	4	39	24
CAG	24	39	4	32	32	4	39	24
ABC	24	39	4	32	32	4	39	24
μ	24	39	4	32	32	4	39	24
σ	0	0	0	0	0	0	0	0

FT = Fault type, μ= Mean absolute squared error, σ = Standard deviation

fault resistance and the fault type (the other parameters were randomly selected).

It can be noticed that for the same fault distance the results are identical and the standard deviation is null, this is due to the fact that the distance directly influences the accuracy of the method. Moreover, it can be seen that the errors are mirrored in the central value of the line, this occurs due to the chosen sampling frequency.

D. GLOBAL RESULTS ANALYSIS

In order to perform a thorough investigation of the proposed method, the authors decided to perform ten thousand simulations where all parameters were randomly selected (fault inception angle, fault resistance, phases involved, and fault distance).

Table 5 presents the results of the proposed method and a comparison to the method presented in [36], where μ is the average fault location absolute error; σ is the standard deviation; ϵ_{min} is the minimum error; and ϵ_{max} is the maximum error.

It can be observed that the proposed method presents a high level of accuracy in all simulations, it also presents a similar behaviour to the method described in [36]. The worst case presents an error of 107 km error and it occurs for a CG fault with fault resistance of 229 Ω and fault inception angle of 245°.

TABLE 5. Global results of the location algorithms.

Method	$\mu\,(m)$	$\sigma\,(m)$	$\epsilon_{\text{min}}\,(m)$	$\epsilon\text{max}\,(m)$
AR[1]	25	13	4	39
EKF[2]	26	16	0	107

[1] Method presented in [36]
[2] Proposed method

Moreover, the global results show that the noninvasive method is robust since the mean absolute error is smaller than the accuracy of the method due to the sampling rate. Thus, better results of the method can only be obtained by increasing the sampling rate, i. e., the method has reached its accuracy limit.

E. QUALITATIVE RESULTS

The proposed method is similar some aspects to the one presented in [36]. The main similarities are:

- Need for time synchronization between both terminals;
- Accuracy limited by sampling frequency;
- Both may detect disturbances, not only faults. Therefore, both need an algorithm for discrimination between these events;
- No need of offline simulations to adjust their coefficients; and
- Slightly sensitive to the spatial position of sensors.

Although there are similarities between them, the positive differences of the proposed method can be highlighted:

- EKF parameters are updated whenever a new magnetic field sample is recorded, therefore, the model adapts itself to different conditions (For example: amplitude, phase and frequency variations for normal operation), avoiding the elaboration of new models (the method presented in [36] needs overtime parameter updating, since the amplitude and the frequency of the system can experience variations);
- Although the model requires a matrix inversion to recalculate its parameters, it can be noticed that since the matrix is single order, as in (15), it presents a low computational cost. The EKF implemented by the authors performs approximately 250 multiplications and 400 additions whenever a new sample is provided by the sensors. This occurs at a sampling rate of 1.5MHz, which means that it is necessary to process around 650MFlops. Currently, this number of operations is not prohibitive and there are several hardware platforms capable of performing them (on the other hand, the method presented in [36] is based on several algorithms that determine the model parameters, including recursive methods that present higher computational costs); and
- The proposed method has a great potential for on-line applications and the disturbance can be located immediately after its occurrence, provided there is communication between both line terminals (the method presented in [36] has a great potential for applications when the focus is to locate only an isolated disturbance in which the system data are saved and post-processed).

V. CONCLUSION

The use of a noninvasive approach to locate faults in transmission lines proved to be a promising alternative, given its capacity to monitor system information from the magnetic field, avoiding the use of conventional VTs and CTs, whose dynamic behaviour may negatively impact fault localization methods.

This work contributed to this research topic, proposing a noninvasive method for fault location in transmission lines, which is based on the Extended Kalman filter (EKF). The proposed method presented encouraging results, since the mean absolute errors found for all simulations were smaller than the error related to the accuracy of the sampling rate. Furthermore, it presented good performance regardless of the parameters that affect the fault waveform. When compared to the method presented in [36], it can be noticed that both have similar proposals, but quite different approaches. The proposed method is self-adapting and do not need to be updated from time to time as the other one. This characteristic makes the proposed method robust for field applications.

It also does not need training procedures, as most of the methods based on machine learning. Besides, the results do not depend on the fault type, resistance, location and inception angle, that usually affects the traditional TW methods. However, it is important to mention that its accuracy is limited by its sampling rate and the use of such technique requires more studies on available hardware technologies, supported by actual field implementations.

REFERENCES

[1] *2020 | State of Reliability: An Assessment of 2019 Bulk Power System Performance*, NERC, North Amer. Electr. Rel. Corp., Atlanta, GA, USA, 2020.

[2] L. de Andrade de Freitas, "A brief history of fault location in transmission lines," in *Proc. 6th IEEE Hist. Electrotechnol. Conf. (HISTELCON)*, Sep. 2019, pp. 44–47.

[3] *IEEE Guide for Determining Fault Location on AC Transmission and Distribution Lines*, IEEE Standard C37.114-2014 (Revision of IEEE Standard C37.114-2004), 2015.

[4] K. Chen, C. Huang, and J. He, "Fault detection, classification and location for transmission lines and distribution systems: A review on the methods," *High Voltage*, vol. 1, no. 1, pp. 25–33, Apr. 2016.

[5] S. Das, S. Santoso, A. Gaikwad, and M. Patel, "Impedance-based fault location in transmission networks: Theory and application," *IEEE Access*, vol. 2, pp. 537–557, 2014.

[6] S. Didehvar and R. M. Chabanloo, "Accurate estimating remote end equivalent impedance for adaptive one-ended fault location," *Electr. Power Syst. Res.*, vol. 170, pp. 194–204, May 2019.

[7] E. K. Mohammedsaeed, M. A. Abdelwahid, and K. Jia, "Distance protection and fault location of the PV power plants distribution lines," *J. Eng.*, vol. 2019, no. 16, pp. 2710–2716, Mar. 2019.

[8] H. K. Jahanger, D. W. P. Thomas, M. Sumner, and C. Rose, "Impact of an inverter-based dg on a double-ended fault location method," *J. Eng.*, vol. 2018, no. 15, pp. 1078–1083, 2018.

[9] M. Ghazizadeh-Ahsaee, "Accurate arcing fault location method for M-terminal transmission lines," *Int. J. Electr. Power Energy Syst.*, vol. 98, pp. 147–155, Jun. 2018.

[10] A. Saber, "New fault location scheme for four-circuit untransposed transmission lines," *Int. J. Electr. Power Energy Syst.*, vol. 99, pp. 225–232, Jul. 2018.

[11] S. Hussain and A. H. Osman, "Fault location scheme for multi-terminal transmission lines using unsynchronized measurements," *Int. J. Electr. Power Energy Syst.*, vol. 78, pp. 277–284, Jun. 2016.

[12] G. Wijaya, A. Suwarno, and A. Abu-Siada, "Review of transmission line fault location using travelling wave method," in *Proc. Conf. Power Eng. Renew. Energy (ICPERE)*, Oct. 2018, pp. 1–6.

[13] A. Di Tomasso, G. Invernizzi, and G. Vielmini, "Accurate single-end and double-end fault location by traveling waves: A review with some real applications," in *Proc. AEIT Int. Annu. Conf. (AEIT)*, 2019, pp. 1–6.

[14] A. Ghaderi, H. A. Mohammadpour, and H. Ginn, "Active fault location in distribution network using time-frequency reflectometry," in *Proc. IEEE Power Energy Conf. Illinois (PECI)*, Feb. 2015, pp. 1–7.

[15] M. A. Aftab, S. M. S. Hussain, I. Ali, and T. S. Ustun, "Dynamic protection of power systems with high penetration of renewables: A review of the traveling wave based fault location techniques," *Int. J. Electr. Power Energy Syst.*, vol. 114, Jan. 2020, Art. no. 105410.

[16] K. Yu, J. Zeng, X. Zeng, F. Xu, Y. Ye, and Y. Ni, "A novel traveling wave fault location method for transmission network based on directed tree model and linear fitting," *IEEE Access*, vol. 8, pp. 122610–122625, 2020.

[17] D. Akmaz, M. S. Mamiş, M. Arkan, and M. E. Tağluk, "Transmission line fault location using traveling wave frequencies and extreme learning machine," *Electr. Power Syst. Res.*, vol. 155, pp. 1–7, Feb. 2018.

[18] L. Rui, L. Chenglei, P. Nan, C. Menghan, and W. Fei, "Fault location for power grid based on transient travelling wave data fusion via asynchronous voltage measurements," *Int. J. Electr. Power Energy Syst.*, vol. 93, pp. 426–439, Dec. 2017.

[19] M. Davoudi, J. Sadeh, and E. Kamyab, "Transient-based fault location on three-terminal and tapped transmission lines not requiring line parameters," *IEEE Trans. Power Del.*, vol. 33, no. 1, pp. 179–188, Feb. 2018.

[20] N. S. Wani, R. Singh, and M. U. Nemade, "Detection, classification and localization of faults of transmission lines using wavelet transform and neural network," *Int. J. Appl. Eng. Res.*, vol. 13, no. 1, pp. 98–106, 2018.

[21] G. K. Purushothama, A. U. Narendranath, D. Thukaram, and K. Parthasarathy, "ANN applications in fault locators," *Int. J. Electr. Power Energy Syst.*, vol. 23, no. 6, pp. 491–506, Aug. 2001.

[22] J. A. O. Neto and M. A. A. Castro, "Classification and localization of high impedance faults in power distribution systems," *Revista Pesquisa Nav.*, vol. 26, no. 1, pp. 56–66, 2014.

[23] J. Liang, T. Jing, H. Niu, and J. Wang, "Two-terminal fault location method of distribution network based on adaptive convolution neural network," *IEEE Access*, vol. 8, pp. 54035–54043, 2020.

[24] C. Fei, G. Qi, and C. Li, "Fault location on high voltage transmission line by applying support vector regression with fault signal amplitudes," *Electr. Power Syst. Res.*, vol. 160, pp. 173–179, Jul. 2018.

[25] R. Rohani and A. Koochaki, "A hybrid method based on optimized neuro-fuzzy system and effective features for fault location in VSC-HVDC systems," *IEEE Access*, vol. 8, pp. 70861–70869, 2020.

[26] I. Kiaei and S. Lotfifard, "A two-stage fault location identification method in multiarea power grids using heterogeneous types of data," *IEEE Trans. Ind. Informat.*, vol. 15, no. 7, pp. 4010–4020, Jul. 2019.

[27] M. Navaei, A. A. Abdoos, and M. Shahabi, "A new control unit for electronic ferroresonance suppression circuit in capacitor voltage transformers," *Int. J. Electr. Power Energy Syst.*, vol. 99, pp. 281–289, Jul. 2018.

[28] Q. Huang, W. Zhen, and P. W. T. Pong, "A novel approach for fault location of overhead transmission line with noncontact magnetic-field measurement," *IEEE Trans. Power Del.*, vol. 27, no. 3, pp. 1186–1195, Jul. 2012.

[29] M. Kazim, A. H. Khawaja, U. Zabit, and Q. Huang, "Fault detection and localization for overhead 11-kV distribution lines with magnetic measurements," *IEEE Trans. Instrum. Meas.*, vol. 69, no. 5, pp. 2028–2038, May 2020.

[30] M. Vopálenskỳ, A. Platil, and P. Kašpar, "Wattmeter with AMR sensor," *Sens. Actuators A, Phys.*, vol. 123, pp. 303–307, Sep. 2005.

[31] C. Reig, M.-D. Cubells-Beltrán, and D. Ramírez Muñoz, "Magnetic field sensors based on giant magnetoresistance (GMR) technology: Applications in electrical current sensing," *Sensors*, vol. 9, no. 10, pp. 7919–7942, Oct. 2009.

[32] J. W. Stahlhut, G. T. Heydt, and E. Kyriakides, "Innovative sensory concepts for power systems," in *Proc. 38th North Amer. Power Symp.*, Sep. 2006, pp. 397–404.

[33] C. Zheng *et al.*, "Magnetoresistive sensor development roadmap (non-recording applications)," *IEEE Trans. Magn.*, vol. 55, no. 4, pp. 1–30, Apr. 2019.

[34] K. Zhu, W. K. Lee, and P. W. T. Pong, "Non-contact capacitive-coupling-based and magnetic-field-sensing-assisted technique for monitoring voltage of overhead power transmission lines," *IEEE Sensors J.*, vol. 17, no. 4, pp. 1069–1083, Feb. 2017.
[35] C. A. F. Sartori and F. X. Sevegnani, "Fault classification and detection by wavelet-based magnetic signature recognition," *IEEE Trans. Magn.*, vol. 46, no. 8, pp. 2880–2883, Aug. 2010.
[36] J. A. O. Neto, C. A. F. Sartori, E. Blanco, and J. Huillery, "Auto-regressive model of magnetic signature for non-invasive fault location in power systems," in *Proc. 11th Latin-Amer. Congr. Electr. Gener. Transmiss.*, no. 1, 2015, p. 165.
[37] M. J. McGrath and C. N. Scanaill, "Key sensor technology components: Hardware and software overview," in *Sensor Technologies*. Springer, 2013, pp. 51–77.
[38] A. Emanuel, J. Orr, D. Pileggi, and E. Gulachenski, "A non-contact technique for determining harmonic currents present in individual conductors of overhead lines," *IEEE Trans. Power App. Syst.*, vol. PAS-102, no. 3, pp. 596–603, Mar. 1983.
[39] A. A. Girgis and E. B. Makram, "Application of adaptive Kalman filtering in fault classification, distance protection, and fault location using microprocessors," *IEEE Trans. Power Syst.*, vol. 3, no. 1, pp. 301–309, Feb. 1988.
[40] P. K. Dash, R. K. Jena, G. Panda, and A. Routray, "An extended complex Kalman filter for frequency measurement of distorted signals," *IEEE Trans. Instrum. Meas.*, vol. 49, no. 4, pp. 746–753, Aug. 2000.
[41] K. Nishiyama, "A nonlinear filter for estimating a sinusoidal signal and its parameters in white noise: On the case of a single sinusoid," *IEEE Trans. Signal Process.*, vol. 45, no. 4, pp. 970–981, Apr. 1997.
[42] R. E. Kalman, "A new approach to linear filtering and prediction problems," *J. Basic Eng.*, vol. 82, no. 1, pp. 35–45, Mar. 1960.
[43] D. H. Boteler, R. J. Pirjola, and L. Marti, "Analytic calculation of geoelectric fields due to geomagnetic disturbances: A test case," *IEEE Access*, vol. 7, pp. 147029–147037, 2019.
[44] L. Trichtchenko and D. H. Boteler, "Effects of recent geomagnetic storms on power systems," in *Proc. 7th Int. Symp. Electromagn. Compat. Electromagn. Ecol.*, Jun. 2007, pp. 265–268.
[45] *Electric Power, Alternating Current MIL-STD-1399*, Standard MIL-STD-1399, Department of Defense Interface Standard Section 300B, United States Department Defense, Apr. 2008.
[46] K. J. Ferreira and A. E. Emanuel, "A noninvasive technique for fault detection and location," *IEEE Trans. Power Del.*, vol. 25, no. 4, pp. 3024–3034, Oct. 2010.
[47] W. I. Bowman and J. M. McNamee, "Development of equivalent pi and t matrix circuits for long untransposed transmission lines," *IEEE Trans. Power App. Syst.*, vol. 83, no. 6, pp. 625–632, Jun. 1964.
[48] F. X. Sevegnani, "Análise da assinatura magnética resultante de faltas em sistemas elétricos via wavelets," Ph.D. dissertation, Departamento de Engenharia de Energia e Automação Elétricas, Universidade de São Paulo, São Paulo, Brazil, 2009.
[49] Q. Huang, R. Yao, F. Li, and W. Zhen, "Design and implementation of a non-contact magnetic field measurement based fault location system for overhead transmission line," in *Proc. IEEE Int. Conf. Smart Instrum., Meas. Appl. (ICSIMA)*, Nov. 2013, pp. 1–4.

JÉSUS ANÍCIO DE OLIVEIRA NETO graduated in electrical engineering from the Universidade Federal de Viçosa, in 2011, and the master's degree in electrical engineering from the Universidade de São Paulo, in 2016, where he is currently pursuing the Ph.D. degree in electrical engineering. He is currently in charge of the Engineering System Development Division and the Head of the Development, Feasibility Studies, and Simulations Section, Navy Nuclear Development Directorate. He has experience in the area of electrical engineering, acting mainly on the following subjects: signal processing, energy distribution systems, biomedical engineering, fault location and classification, and electromagnetic compatibility.

CARLOS ANTONIO FRANCA SARTORI (Senior Member, IEEE) received the B.Sc., M.Sc., and Ph.D. degrees in electrical engineering from the Escola Politécnica, University of São Paulo (EPUSP), in 1983, 1994, and 1999, respectively. He worked at the National Commission on Nuclear Energy CNEN/IPEN-SP (1984–2018), where he was the technical lead responsible of the Electromagnetic Compatibility (EMC) Group. He is an Invited Professor with the Graduated Programs of EPUSP (1999) and at the Nuclear and Energy Research Institute IPEN-CNEN/SP (2006), and an Associate Professor at the Catholic University of São Paulo (PUC/SP), where he was the Vice-Head of the Department of Electrical Engineering (1997–1998), and the Vice-Dean (2001–2004). He has coauthored more than 100 articles. He is the South Brazil IEEE EMC Chapter Chair, and a former IEEE EMC Board of Director Member. He is also a member of the International Compumag Society (ICS) and of the Brazilian Society on Electromagnetics (SBMAG), where he was the Vice-President (1998–2002).

GIOVANNI MANASSERO JUNIOR (Member, IEEE) received the B.Sc., M.Sc., and Ph.D. degrees from the Universidade de São Paulo, São Paulo, Brazil, in 1999, 2001, and 2006, respectively. He joined the Universidade de São Paulo, in 2009, where he is currently an Assistant Professor with the Electric Energy and Automation Engineering Department. His research fields include power systems protection, modeling, and simulation.